

Optimal Design of Nonlinear Multimaterial Structures for Crashworthiness Using Cluster Analysis

Kai Liu

Ph.D. Candidate
School of Mechanical Engineering
Purdue University
West Lafayette, Indiana, USA
liu915@purdue.edu

Duane Detwiler

Honda R&D Americas, Inc.
Chief Engineer, Vehicle Research - CAE
Manager, Strategic Research Department 1 (SR1)
Raymond, Ohio, USA
ddetwiler@oh.hra.com

Andres Tovar*

Associate Professor, Member of ASME
Department of Mechanical Engineering
Indiana University-Purdue University Indianapolis
Indianapolis, Indiana, USA
tovara@iupui.edu

This study presents an efficient multimaterial design optimization algorithm that is suitable for nonlinear structures. The proposed algorithm consists of three steps: conceptual design generation, clustering, and metamodel-based global optimization. The conceptual design is generated using a structural optimization algorithm for linear models or a heuristic design algorithm for nonlinear models. Then, the conceptual design is clustered into a predefined number of clusters (materials) using a machine learning algorithm. Finally, the global optimization problem aims to find the optimal material parameters of the clustered design using metamodels. The metamodels are built using sampling and cross-validation, and sequentially updated using an expected improvement function until convergence. The proposed methodology is demonstrated using examples from multiple physics and compared with traditional multimaterial topology optimization method. The proposed approach is applied to nonlinear, multi-objective design problems for crashworthiness.

1 Introduction

Multimaterial structural optimization has the potential to synthesize structures of higher performance than the ones obtained with traditional binary-phase (solid-void) topology optimization methods. With the increasing availability of multimaterial additive manufacturing technologies, multimaterial topology optimization also becomes increasingly relevant.

Most of the available multimaterial topology optimization methods fall into one of the following classes: homogenization design method, density-based method, level set-based method, phase field-based method, and heuristic methods. Homogenization design methods assume that the structure is composed of a periodically perforated microstructure, so its bulk mechanical properties can be determined using homogenization theory [1,2]. The main drawback of this approach is that the optimal microstructure, which may change at every point within the structure, is not always known. This can be alleviated by restricting the method to a subclass of microstructure. This approach, referred to as partial relaxation, has been used to generate conceptual designs of three-phase material composites with extremal thermal expansion

*Address all correspondence to this author.

[3], piezoelectricity [4], and bulk modulus [5]. An additional problem with the homogenization methods is the manufacturability of the optimized structure. The microscopic holes in the microstructure may be difficult or impossible to fabricate.

Density-based methods are an alternative that avoids the application of homogenization theory by using a continuous density value without a microstructure. In a discretized design domain, the mechanical properties of the material element (stiffness tensor coefficients) are determined according to a rule of mixture between two phases using a power-law interpolation function [6,7]. When only a two-phase material design is considered, the power law may implicitly penalize intermediate density values driving the structure towards a binary configuration. The use of such a penalization procedure is referred to as the Solid Isotropic Material with Penalization (SIMP) method [8]. For a three-phase material design the rule of mixtures can be easily extended. Due to its simplicity, the SIMP method has been extensively used in multimaterial topology optimization [9–11]. The effective use of the SIMP-based methods requires regularization procedures such as filters, which are purely heuristic and very sensitive to changes.

Alternatives to the density-based methods are the level set-based methods and the phase field-based methods. The level set-based methods use implicit iso-contours of a level-set function to define the boundaries between material phases. In this sense, these are related to shape optimization methods. These methods avoid the use of filters and other regularization procedures used in density-based methods and have become popular in structural topology optimization [12–14]. The level-set method has been extended to multimaterial topology optimization following two main approaches: the extended variational multilevel sets approach [15–19] and the extended piecewise-constant variational level set approach [20, 21]. Recently, Kriging metamodels have been also incorporated in level set-based topology optimization [22–24]. The automatic changes of the topology through breaking and merging also require the level-set function to be re-initialized during the update operation in order to achieve appropriate numerical accuracy. Although several attempts have been reported to address this issue [25–28], the re-initialization operation still relies on heuristics.

Phase field-based methods are free boundary tracking methods that avoid the need for re-initialization [29–34]. These methods are capable of handling the motion caused by domain states and the motion caused by the domain shape, e.g., the temperature and the mean curvature motion, respectively, so they are also related to shape optimization methods. Unfortunately, these methods are not easily extended to nonlinear problems involving contact, large displacements, and plasticity.

Outstanding heuristic approaches for multimaterial topology optimization are the bi-directional evolutionary structural optimization (BESO) method [35,36], the Discrete Material Optimization (DMO) method [37, 38], and the Hybrid Cellular Automaton (HCA) method [39, 40]. For in-

stance, HCA can be efficient in problems involving a large number of design variables in nonlinear multimaterial structures [41]; however, heuristic methods are not applicable to general structural optimization problems.

Recently, clustering or related techniques have been explored in topology optimization to reduce the computational cost of the optimization algorithm or to reduce the dimension of the design space. Using a modified P-norm distance, stress functions have been grouped to reduce the number of constraints in stress-constrained topology optimization [42]. A clustering method in a genetic algorithm is also being reported for the design of rotor topologies [43, 44]. Clustering in topology optimization has been utilized by researchers at the Honda Research Institute Europe GmbH to reduce the dimension in a (multi-dimensional) local state features space [45]. Finally, in our previous work [46], K-means clustering is tailored to reduce the dimension of the design space and allow the application of a heuristic multiobjective, metamodel-based optimization algorithm. This approach has been developed over the years and the current state is summarized in this work.

Here, we propose a method for multimaterial structure optimization that incorporates clustering and is suitable to efficiently solve large-scale optimization problems involving nonlinear structures. The resulting structures are well-defined multimaterial designs without artificial (intermediate) materials. The proposed design optimization algorithm consists of three steps: conceptual design generation, design clustering, and metamodel-based global optimization. During the first step, the conceptual design is generated using a structural optimization algorithm for linear models or a heuristic design algorithm, such as HCA, for nonlinear models. During the second step, the dimensionality of the problem is reduced by clustering the continuous field variable. To this end, unsupervised machine learning, i.e., K-means clustering, is implemented to optimally group the continuous field variable into a reduced number of clusters. The number of clusters determines the number of materials within the structure. During the third step, metamodels are built using appropriate curve fitting or interpolation functions, e.g., Kriging metamodels. Then, the metamodels are sequentially updated using an expected improvement function. The global optimum, which corresponds to the present best function value, is obtained once the expected improvement reaches a sufficiently small value.

2 Conceptual Design

The first step of the proposed design strategy is to generate a conceptual multimaterial design of the structure. If the structure's finite element model is linear and numerically tractable, a structural optimization algorithm can be used to generate the conceptual design. Otherwise, a heuristic design algorithm can be used instead. The heuristic design algorithm used in this work is HCA [39]. HCA is commercially available in LS-TaSC for LS-DYNA (LSTC, California). In either case, the material property is characterized by the design variable $x_e \in \mathbb{R}$, where $0 \leq x_e \leq 1$, for $e = 1, \dots, n$, where

n is the number of finite elements in the structure's finite element model. The conceptual design problem is to find the distribution of all possible materials $\mathbf{x} \in \mathbb{R}^n$ that minimize the objective function $f(\mathbf{x}) : \mathbb{R}^n \rightarrow \mathbb{R}$ subjected to a set of (equality and inequality) constraints. The optimization problem is expressed as:

$$\begin{aligned} & \text{find } \mathbf{x} \in \mathbb{R}^n \\ & \text{minimize } f(\mathbf{x}, \mathbf{U}(\mathbf{x}, t)) \\ & \text{subject to } \mathbf{h}(\mathbf{x}, \mathbf{U}(\mathbf{x}), t) = \mathbf{0} \\ & \quad \mathbf{g}(\mathbf{x}, \mathbf{U}(\mathbf{x}), t) \leq \mathbf{0} \\ & \quad 0 \leq x_e \leq 1, \quad e = 1, \dots, n, \end{aligned} \quad (1)$$

satisfying the finite element equilibrium equations. If the problem involves microstructured multi-phased isotropic materials, then it must also consider limits such as the Hashin-Shtrikman bounds [47]. It becomes apparent that the mapping between the design variable x_e and the material property must be correctly selected in order to avoid a non-physical distribution of artificial materials.

Representing the material property by a single scalar is generally possible with the use of homogenization methods. In that way, two or multiple phases are blended to form a new (composite) material. To generate the conceptual design, this work makes use of a linear interpolation:

$$\mathbf{P}_e = \mathbf{P}_{\min} + (\mathbf{P}_0 - \mathbf{P}_{\min})x_e, \quad (2)$$

where \mathbf{P}_e is the element material property tensor. The optimal material distribution (or an approximation) $\mathbf{x}^* \in \mathbb{R}^n$ from Eq. (1) is used as the conceptual design. Generally, the desired number of materials K in the final design is significantly smaller than n —the value of n is in the order of 10^3 to 10^6 . Therefore, the dimension of the problem is reduced by mapping the n optimal values into K clusters as described in Sec. 3.

3 Clustering

The dimension reduction problem consists on drawing inferences from datasets consisting of input data without labeled responses. The solution to this problem, usually addressed by cluster analysis in unsupervised machine learning, leads to groups of observations in such a way that the observations in the same group are more similar to each other than to those in other groups. Cluster analysis has been used in global optimization to identify promising design regions [48] and eliminate near-duplicate designs [49]. In contrast to this prevailing use, this work applies cluster analysis to downsize the dimension of the design space reducing the number of the materials from the conceptual design.

Due to its effectiveness and simplicity, K-means is one of the most popular and widely used cluster analysis algorithms [50]. K-means cluster analysis is employed in this work. The input to this cluster analysis algorithm is a set of

n observations and the desired number of clusters K , where $1 \leq K \leq n$; usually, $K \ll n$. In this application, an observation consists of a single attribute, namely, the normalized material parameter x_e , where $0 \leq x_e \leq 1$ and $e = 1, \dots, n$. A discussion on the optimal value of K can be found in [51].

To start the clustering process, the algorithm distributes K cluster seeds within the set of all observations x_e , where $e = 1, \dots, n$. According to the distance between the observations and each seed, the set is partitioned into Voronoi cells (clusters) S_k , where $k = 1, \dots, K$. From this point, the algorithm finds the cluster centroid values μ_k that minimize the within-cluster sum of squares. Mathematically, this problem is expressed as follows:

$$\begin{aligned} & \text{find } \boldsymbol{\mu} \in \mathbb{R}^K \\ & \text{minimize } J(\boldsymbol{\mu}) = \sum_{k=1}^K \sum_{x_e \in S_k} (x_e - \mu_k)^2. \end{aligned} \quad (3)$$

In order to solve the clustering problem in Eq. (3), an iterative refinement algorithm is utilized [52] (Algorithm 1). Due to the nonlinearity of the optimization problem, the final clustering depends heavily on the initial cluster seed distribution. While global optimization methods may be suitable, this work addresses this limitation by using 1000 randomly-generated initial seeds. After the clustering, the value of $x_e \in S_k$ is replaced by μ_k . The result is a K -dimensional clustered design suitable for building metamodels and performing global optimization. The computational cost of solving Eq. (3) is usually a small fraction of the cost of a finite element analysis.

Algorithm 1: Iterative K-means clustering algorithm:

```

1 Randomly initialize  $K$  cluster centroids,  $\mu_1, \dots, \mu_K$ ;
2 while stopping criterion has not been met do
3   for  $k : 1$  to  $K$  do
4      $S_k \leftarrow \{\}$ ;
5   end
6   for  $e : 1$  to  $n$  do
7      $j \leftarrow \operatorname{argmin}_j (x_e - \mu_j)^2$ ;
8      $S_j \leftarrow S_j \cup \{x_e\}$ ;
9   end
10  for  $k : 1$  to  $K$  do
11     $\mu_k \leftarrow \frac{1}{|S_k|} \sum_{x_e \in S_k} x_e$ ;
12  end
13 end

```

A rigorous method to find K has not yet found and, therefore, a parametric study is utilized as shown in the numerical examples (Secs. 6.3 and 6.4). The metamodel-based global optimization strategy presented in this work consists of two steps: generating initial metamodels via sampling and cross-validation (Sec. 4), and finding the global optimum design via expected improvement maximization (Sec. 5).

4 Generation of the Initial Metamodels

Dynamic models involving geometric, material, and contact nonlinearities are commonly found in crash simulations [53]. For such models, the computational cost of a function evaluation is considerably high and it is impractical to use traditional gradient-based optimization methods due to the lack of reliable sensitivity coefficients. As an alternative, metamodels can be derived by sampling the dynamic, nonlinear finite element model. The resulting metamodels are numerically inexpensive and allow to find near-optimal solutions through the use of global multi-objective algorithms [51]. The key aspect to using metamodels for global optimization lies in balancing between global exploration and local exploitation. It is desirable to generate an accurate metamodel that explores a large portion of the design space with a few sampling points.

Several metamodels have been evaluated for design problems in crashworthiness including: polynomial response surface, radial basis functions, and Kriging [51]. Based on cross-validation errors, Kriging is the preferred metamodel and it is used in this work. The general form of the Kriging metamodel \hat{f} is of a function f is

$$\hat{f}(\mathbf{S}) = \mathbb{E}[\hat{f}(\mathbf{S})] + \sum_{p=1}^P \omega_p \left\{ f(\mathbf{S}^{(p)}) - \mathbb{E}[f(\mathbf{S}^{(p)})] \right\} \quad (4)$$

where $\mathbb{E}[\cdot]$ is the expected value (mean), $\mathbf{S}^{(p)}$ are the p th sampled designs, and ω_p are the Kriging weights, which are derived from a covariance function. This metamodel can be found implemented in MATLAB [54]. One metamodel is built for each function in the optimization problem.

4.1 Sampling

Computer design of experiments is the selection procedure for finding the points in the design space that must be simulated. Many strategies can be used to sample the design points including factorial designs, D-optimal designs, and Latin hypercube sampling (LHS) [55]. LHS is used in this work to generate the initial metamodel. This provides designs that are independent of the mathematical model of the approximation and allow the estimation of the main effects of all factors in the design in an unbiased manner. Another advantage of LHS is the number of points to be evaluated can be directly defined. For K clusters (design variables) and P design points, the LHS provides a $P \times K$ matrix \mathbf{S} that randomly samples the entire design space broken down into P equal-probability regions. The LHS matrix components are defined as

$$S_{pk} = \frac{\eta_{pk} - 0.5}{P}, \quad (5)$$

where $\eta_{1k}, \dots, \eta_{pk}$ are uniform random permutations of the integers 1 through P . However, the LHS design points generated using Eq. 5 might be highly correlated, which is undesirable (Fig. 1a). Approaches to avoid high correlation in-

cluding correlation minimization methods [56] and the maximization of the minimum inter-site distances [57]. The later one is used in this work. In this approach, the inter-site distance between two samples $\mathbf{S}^{(r)}$ and $\mathbf{S}^{(t)}$ is defined as

$$d(\mathbf{S}^{(r)}, \mathbf{S}^{(t)}) = \left[\sum_{j=1}^K (S_{rk} - S_{tk})^2 \right]^{1/2}, \quad (6)$$

for $r, t \in \{1, 2, \dots, P\}$, where $\mathbf{S}^{(r)}$ is the r th row of the sampling matrix \mathbf{S} , and S_{rk} indicates the k th column of the row vector $\mathbf{S}^{(r)}$. Figure 1b shows an optimal LHS generated from the use of the maximize the minimum inter-site distance criterion.

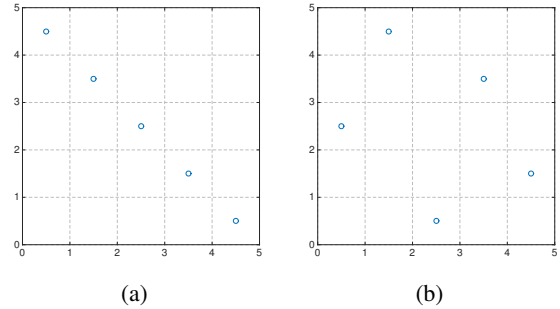


Fig. 1: Latin hypercube samplings with $P = 5$ and (a) high correlation and (b) low correlation achieved using the maximization of the minimum inter-site distances.

4.2 Cross-validation

Despite the number and optimal distribution of the sampled designs, the resulting metamodel may not be sufficiently accurate to provide meaningful predictions. To estimate the accuracy of the metamodel, this work uses the leave-one-out cross-validation. In this cross-validation approach, one design is left out from the P sampled designs; then, the metamodel is re-generated using the remaining $P - 1$ designs (Fig. 2). If $\mathbf{S}^{(p)}$ is the p th sampled design that has been left out, $f(\mathbf{S}^{(p)})$ the function value, and $\hat{f}_{-p}(\mathbf{S}^{(p)})$ is the cross-validated prediction of $f(\mathbf{S}^{(p)})$, then one can plot $\hat{f}_{-p}(\mathbf{S}^{(p)})$ against $f(\mathbf{S}^{(p)})$. If the metamodel fits perfectly, these points should lie on the 45° line [58]. If this diagnostic plot looks satisfactory, e.g., high coefficient of determination R^2 , then the metamodel is also considered satisfactory; otherwise, the metamodel is refit with a log or inverse transformation to the dependent variable. If one of these transformations gives satisfactory diagnostic plot, then this transformation function is used in the rest of the analysis.

In addition, root-mean-square error (RMSE) from the predicted residual error sum of squares (PRESS) vector can be used to estimate the cross-validation error. Using the leave-one-out cross-validation, the PRESS vector \mathbf{e} is formed with the errors $e_p = |f(\mathbf{S}^{(p)}) - \hat{f}_{-p}(\mathbf{S}^{(p)})|$ obtained when the

p th sampled design is left out. Then, the RMSE from the PRESS vector is given by [59]:

$$\text{PRESS}_{\text{RMS}} = \sqrt{\frac{1}{P} \mathbf{e}^T \mathbf{e}}. \quad (7)$$

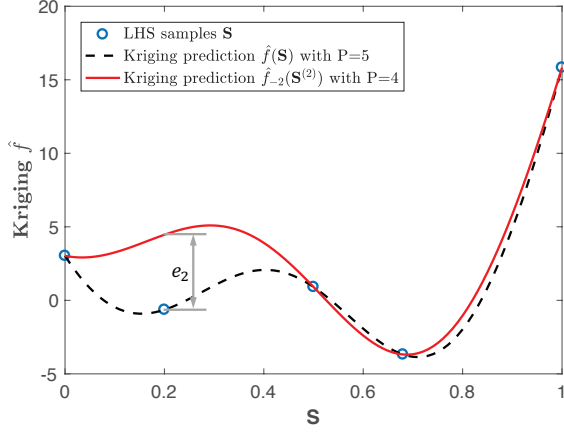


Fig. 2: Leave-one-out cross-validation at the second sampled point exemplified by fitting a function with a Kriging meta-model.

5 Metamodel-based Global Optimization

Once the initial metamodels are built, the global optimization problem can be solved. The global optimization problem is to find the material parameters that minimize the objective function vector $\mathbf{f}(\boldsymbol{\mu}) : \mathbb{R}^K \rightarrow \mathbb{R}^{n_f}$, where n_f is the number of objective functions. The input to the metamodels $\hat{\mathbf{f}}$ is the vector of clustered design variables $\boldsymbol{\mu}$. The output is the predicted values of the finite element models \mathbf{f} . The optimal design can be found using the Efficient Global Optimization (EGO) algorithm [58, 60]. During the search for the global optimum, the EGO algorithm balances between global exploration and local exploitation.

5.1 Expected Improvement

The expected improvement function calculates the amount of improvement one can expect at a given point $\mathbf{S}^{(p)}$. The expected improvement function is defined as

$$\mathbb{E}[I(\mathbf{S}^{(p)})] = \mathbb{E}[\max(f_{pbs} - F, 0)], \quad (8)$$

where $f_{pbs} = \min\{f(\mathbf{S}^{(1)}), \dots, f(\mathbf{S}^{(p)}), \dots, f(\mathbf{S}^{(P)})\}$ is the present best function value (pbs) and F is a normally distributed random variable with mean and standard deviation defined by the Kriging metamodel. With $F \sim \mathcal{N}(\hat{f}, \sigma^2)$, one can express the expected improvement as follows [58]:

$$\mathbb{E}[I(\mathbf{S}^{(p)})] = (f_{pbs} - \hat{f}) \Phi(u) + \sigma(\mathbf{S}^{(p)}) \phi(u), \quad (9)$$

where $u = (f_{pbs} - \hat{f}) / \sigma$, $\hat{f} = \hat{f}(\mathbf{S}^{(p)})$ is the predicted value at point $\mathbf{S}^{(p)}$, $\sigma^2(\mathbf{S}^{(p)})$ is the variance of the Kriging predictor, and $\Phi(\cdot)$ and $\phi(\cdot)$ are the cumulative density function (CDF) and probability density function (PDF) of a normal distribution, respectively.

For constrained problems, one must ensure the feasibility of the newly selected points $\mathbf{S}^{(p)}$. If the finite element model used to evaluate the constraint is computationally expensive, the constraint can be approximated using a meta-model. In this case, the probability of feasibility needs to be considered along with the expected improvement on the objective function [60]. If the new point is not feasible, its corresponding expected improvement must be zero.

The expected improvement function is maximized using an evolutionary algorithm or a branch-and-bound algorithm. If the maximum expected improvement is less than 0.1% of the present best function value in two consecutive iterations, then convergence is achieved and the metamodel needs no further improvement; otherwise, the point where the expected improvement is maximized is added to the sampled set and the metamodel is updated. If no convergence is achieved in 100 iterations, the algorithm is terminated.

5.2 Multi-objective Expected Improvement

For a multi-objective optimization problem, a multi-objective expected improvement function needs to be defined. Consider an optimization problem that minimizes two objectives $f_1(\mathbf{x})$ and $f_2(\mathbf{x})$, with the set of m Pareto points

$$\mathbf{f}_{1,2}^* = \left\{ \left(f_1^{*(1)}, f_2^{*(1)} \right), \dots, \left(f_1^{*(m)}, f_2^{*(m)} \right) \right\}, \quad (10)$$

where $f_j^{*(i)} = f_j(\mathbf{S}^{*(i)})$ and $\mathbf{S}^{*(i)}$ is a Pareto design. The expected improvement for this multi-objective problem is defined as [60]:

$$\mathbb{E}[I(\mathbf{S}^{*(p)})] = \mathbb{P}[I(\mathbf{S}^{*(p)})] \min\{d_1, \dots, d_m\}, \quad (11)$$

where $\mathbb{P}[I(\mathbf{S}^{*(p)})]$ is the probability of improving both functions f_1 and f_2 at the Pareto design $\mathbf{S}^{*(p)}$. The probability of improvement is defined as:

$$\mathbb{P}[I(\mathbf{S}^{*(p)})] = \Phi(u_1^i) + \sum_{i=1}^{m-1} [\Phi(u_1^{i+1}) - \Phi(u_1^i)] \Phi(u_2^{i+1}) + [1 - \Phi(u_1^m)] \Phi(u_2^m), \quad (12)$$

where $u_j^i = u_j^i(\mathbf{S}^{*(p)}) = (f_j^{*(i)} - \hat{f}_j(\mathbf{S}^{*(p)})) / \sigma_j(\mathbf{S}^{*(p)})$.

In Eq. (11), d_i for $i = 1, \dots, m$ is the distance between the vectors (\bar{F}_1, \bar{F}_2) and $(f_1^{*(i)}, f_2^{*(i)})$, where (\bar{F}_1, \bar{F}_2) is the cen-

triod of the probability integral used to calculate $E[I(\mathbf{S}^{*(p)})]$:

$$\bar{F}_1(\mathbf{S}^{*(p)}) = \frac{1}{P[I(\mathbf{S}^{*(p)})]} \left[z_1^1 + \sum_{i=1}^{m-1} (z_1^{i+1} - z_1^i) \Phi(u_2^{i+1}) + z_1^m \Phi(u_2^m) \right] \quad (13)$$

where $z_j^i = z_j^i(\mathbf{S}^{*(p)}) = \hat{f}_j(\mathbf{S}^{*(p)})\Phi(u_j^i) - \sigma_j(\mathbf{S}^{*(p)})\phi(u_j^i)$. $\bar{F}_2(\mathbf{S}^{*(p)})$ is defined similarly. Details on the derivation of the multi-objective expected improvement formula can be found in [60]. The use of the multi-objective expected improvement is illustrated in Secs. 6.3 and 6.4.

6 Numerical Examples

Four examples with different physics are presented in this section. The first two examples involve linear finite element models under a static load and the evaluation of thermal and mechanical compliance. The last two examples involve nonlinear finite element models under a dynamic load (armor plate and vehicle S-rail structure).

In the first two examples, the results are compared with an alternative optimization method, i.e., the alternating active-phase multimaterial topology optimization algorithm [61], which is available in MATLAB. In the last two examples, a parametric study on the number of clusters is included.

6.1 Thermal Compliance

The minimum thermal compliance example is adopted from [61]. The design problem is illustrated in Fig. 3. Due to the axis symmetry of the model, only a quarter of the design domain is considered. The reduced design domain is discretized into 50×50 Q4 elements. The remainder of this section follows the proposed three-step design optimization approach (3SDO).

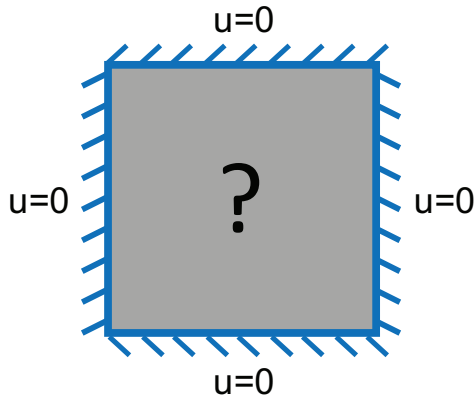


Fig. 3: Thermal compliance problem—Design domain and Dirichlet boundary condition: constant surface temperature $u = 0$.

Step 1: Conceptual design Without a constraint in the number of materials, the optimization problem is stated as follows:

$$\begin{aligned} & \text{find } \mathbf{x} \in \mathbb{R}^n \\ & \text{minimize } f(\mathbf{x}, \mathbf{U}(\mathbf{x})) = \mathbf{F}^T \mathbf{U}(\mathbf{x}) \\ & \text{subject to } h(\mathbf{x}) = \frac{1}{n} \sum_{e=1}^n x_e - m_f = 0 \\ & \quad 0 \leq x_e \leq 1, \quad e = 1, \dots, n, \end{aligned} \quad (14)$$

where $\mathbf{U}(\mathbf{x}) = \mathbf{K}(\mathbf{x})^{-1} \mathbf{F}$ under plane stress. f is the thermal compliance function, $\mathbf{U}(\mathbf{x})$ denotes the finite element global nodal temperature vector, \mathbf{F} denotes the global thermal load vector, and $\mathbf{K}(\mathbf{x})$ denotes the global thermal conductivity matrix. A relative thermal conductivity of 1.0 is defined for the most dense material and 10^{-3} for the least dense material. The element conductivity matrix is interpolated using Eq.(2). The mass constraint limit (or mass fraction) is prescribed to be $m_f = 0.4$. The conceptual design is generated using topology optimization and achieved in 20 iterations. The convergence criterion is $\|\mathbf{x}^k - \mathbf{x}^{k-1}\| \leq 10^{-3}$, where k is the iteration number. The corresponding objective value is $f = 1.94 \times 10^6$. The conceptual design is shown in Fig. 4.

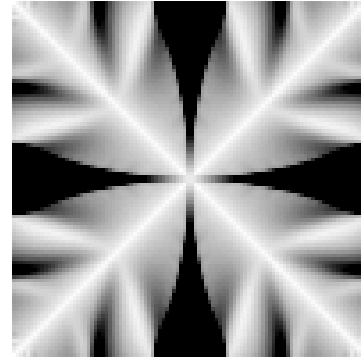


Fig. 4: Thermal compliance problem—Conceptual design with $f = 1.94 \times 10^6$.

Step 2: Clustered design In this example, let us consider four clusters, this is $K = 4$. The K-means clustering optimization in Eq. (3) leads to the optimal material parameters μ_k and corresponding volume fractions m_{fk} summarized in Table 1, for clusters $k = 1, \dots, 4$. The corresponding value of the thermal compliance is $f = 1.97 \times 10^6$. The clustered design is shown in Fig. 5.

Step 3: Metamodel-based global optimization Given the initial material parameters μ_k , for $k = 1, \dots, 4$, the final opti-

Table 1: Thermal compliance problem—Optimal material parameters of the clustered design.

k	Color	μ_k	m_{fk}
1	Red (■)	0.98	0.19
2	Green (■)	0.31	0.30
3	Blue (■)	0.57	0.13
4	Black (■)	0.13	0.38

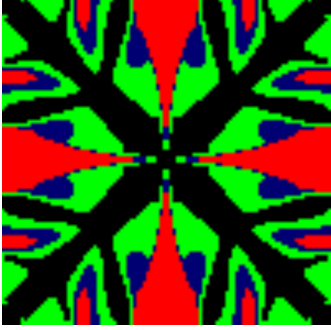


Fig. 5: Thermal compliance problem—Clustered design with $f = 1.97 \times 10^6$.

mization problem is the following:

$$\begin{aligned}
 & \text{find } \boldsymbol{\mu} \in \mathbb{R}^K (K = 4) \\
 & \text{minimize } f(\mathbf{x}(\boldsymbol{\mu})) = \mathbf{F}^T \mathbf{U}(\mathbf{x}(\boldsymbol{\mu})) \\
 & \text{subject to } h(\mathbf{x}(\boldsymbol{\mu})) = \frac{1}{n} \sum_{k=1}^K \sum_{x_e \in S_k} \mu_k - m_f = 0 \quad (15) \\
 & \quad 0.10 \leq \mu_k \leq 1.00, \quad k = 1, \dots, 4,
 \end{aligned}$$

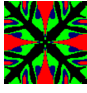

where $x_e = \mu_k$ for all $x_e \in S_k$. The mass function h is linear and no metamodel is required. A Kriging metamodel is built only for the thermal compliance f using the method described in Sec. 4. The Kriging metamodel is trained with 40 samples generated by an optimal Latin hypercube sampling. In this initial metamodel, $R^2 = 0.98$ and $\text{PRESS}_{\text{RMS}} = 0.078$. The constrained expected improvement function is used to search for the global optimum using the EGO algorithm. Converges is achieved in four iterations. In the final metamodel, $R^2 = 0.99$ and $\text{PRESS}_{\text{RMS}} = 0.054$. The optimal material parameters $\mu_1^* = 1.00$, $\mu_2^* = 0.33$, $\mu_3^* = 0.43$, and $\mu_4^* = 0.16$ as summarized in Table 2. The objective value is improved to $f = 1.96 \times 10^6$.

For comparison, this problem is also solved using the alternating active-phase multimaterial topology optimization (MTOP) algorithm [61]. The MTOP algorithm consists of outer and inner iterations. Each outer iteration involves the solution of $K(K-1)/2$ alternating active-phase inner iterations, i.e., binary topology optimization subproblems. It also

requires the definition of the number of materials and their corresponding material properties.

Table 2 summarizes the results obtained by the MTOP algorithm and the proposed three-step design optimization method (3SDO). Both results have the same material parameters $\boldsymbol{\mu}_k^*$ and mass fractions $\mathbf{m}_{\mu k}^*$. As stated in [61], the filter is a key success of the optimization procedure and should be gradually reduced during the multimaterial topology optimization; hence, the filter is applied and gradually reduced in MTOP. A penalization power is also utilized. As it can be seen in Table 2, although the solutions from two different approaches have similar objective value, the structures are quite different. Due to the use of alternative phases, design space dimension \mathbb{R} is considerable higher than the proposed 3SDO method.

Table 2: Thermal compliance problem—Comparison of the final objective value.

	f^*	$\boldsymbol{\mu}_k^*$	$\mathbf{m}_{\mu k}^*$	\mathbb{R}
	1.96×10^6	■ 1.00	■ 0.19	4
3SDO		■ 0.33	■ 0.30	
	1.95×10^6	■ 0.43	■ 0.13	
MTOP		■ 0.16	■ 0.38	2672

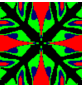

Using the proposed 3SDO approach, the objective function is evaluated only at the conceptual design generation and the metamodel-based global optimization. The conceptual design is generated in 20 topology optimization iterations. The metamodel is built with 40 training samples initially, and converged in four iterations. On the other hand, the MTOP converged in 156 outer iterations, which requires 936 alternating active-phase (inner) iterations. Each inner iteration evaluate the objective function twice. Therefore, the total number of function evaluations for MTOP is $156 \times 6 \times 2 = 1872$. Table. 3 summarizes the number of iterations (# iter) and the computational cost in number of functional evaluations (# feval) in every step of the 3SDO method and the MTOP algorithm.

Scalability The scalability of the optimization method can be assessed from the number of function evaluations. For the proposed 3SDO, the number of function evaluations is given by

$$N_{3SDO} = N_c + N_s K + N_e, \quad (16)$$

where N_c is the number of function evaluations in conceptual design step. $N_s K$ is the initial function evaluations to

Table 3: Thermal compliance problem—Comparison of the computational cost.

	Step	# iter	# feval
	1. Conceptual	20	20
	2. Clustering	7	0
3SDO	3a. Sampling	40	40
	3b. Optimization	4	4
	Outer	156	0
MTOP	Inner	936	1872

generate the metamodel and N_e is the number of function evaluations in the EGO.

On the other hand, the number of function evaluations for the MTOP is given by

$$N_{MTOP} = N_o \times K \times (K - 1), \quad (17)$$

where N_o is the outer iteration number. From Eq. (16) and Eq. (17), the proposed 3SDO method is linear with number of clusters K while the MTOP is quadratic with K . A plot of number of function evaluations with up to 10 materials is given in Fig. 6 with $N_c = 100, N_s = 10, N_e = 100$ and $N_o = 500$.

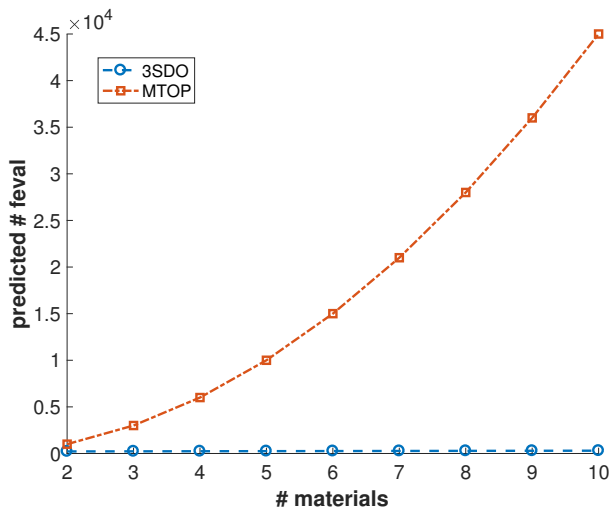


Fig. 6: Thermal compliance problem—Comparison of the predicted number of function evaluations.

6.2 Mechanical Compliance under a Static Load

Let us consider the optimal distribution of three different materials ($K = 3$) in a 3D beam in cantilever (Fig. 7). The objective is to minimize the mechanical compliance subjected

to a mass constraint. The design domain is discretized into $60 \times 20 \times 8$ H8 identical finite elements. The three-step design optimization approach is applied as follows.

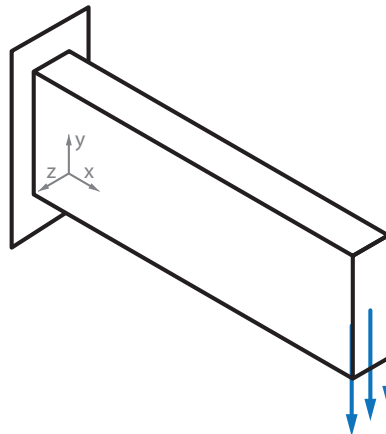


Fig. 7: Mechanical compliance problem—Design domain and boundary conditions for the 3D beam in cantilever.

Step 1: Conceptual design The mechanical compliance is a scalar counterpart of thermal compliance. The optimization problem is stated as in Eq. (14) except that $\mathbf{U}(\mathbf{x})$ is the nodal displacement vector, \mathbf{F} is the external load vector, and $\mathbf{K}(\mathbf{x})$ is the stiffness matrix. The mass fraction constraint is prescribed to be $m_f = 0.3$. The relative elastic modulus of the most dense material is 1.0 and the one of the least dense material is 10^{-3} . The Poisson's ratio is 0.3.

The optimal density distribution \mathbf{x}^* (Fig. 8) is achieved in 64 iterations using Top3d [62] with a control-based strategy [63]. The convergence criterion is $\|\mathbf{x}^k - \mathbf{x}^{k-1}\| \leq 10^{-3}$, where k is the iteration number. The optimal design variables are distributed from 1.0 (stiff material in black color) to 0.0 (compliant material in white color) with 8320 distinct values (using 16 digits of precision). The corresponding objective function value is $f = 2217$.

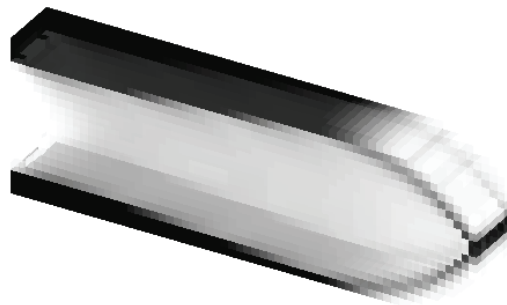


Fig. 8: Mechanical compliance problem—Conceptual design with 8320 distinct density values and $f = 2217$.

Step 2: Clustered design The conceptual design is then clustered into three clusters (Fig. 9). As in the previous example, contour indicates the cluster distribution. The clustered design has compliance value $f = 2432$, which is, as expected, higher than the one of the conceptual design.

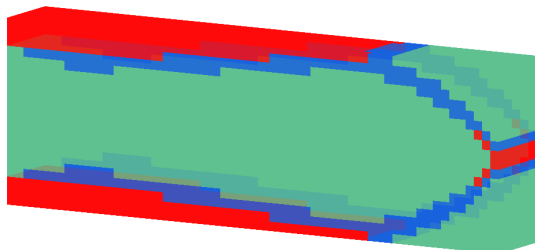


Fig. 9: Mechanical compliance problem—Clustered design with three clusters and $f = 2432$.

Step 3: Metamodel-based global optimization The optimization problem is to minimize mechanical compliance subject to a mass constraint with three design variables. The initial Kriging metamodel of the mechanical compliance is built with 30 LHS samples. In this metamodel, $R^2 = 0.99$ and $PRESS_{RMS} = 0.037$. The final design is obtained after three EGO iterations using the constrained expected improvement function. In the final metamodel, $R^2 = 0.99$ and $PRESS_{RMS} = 0.034$. The comparison between 3SDO and MTOP on the final objective value and computational cost is summarized in Tables 4 and 5, respectively. Results demonstrate the effectiveness and efficiency of the proposed algorithm: the 3SDO requires only 3% of functional evaluation and it is able to achieve result 11% better than the MTOP.

Table 4: Mechanical compliance problem—Comparison of the final objective value.

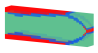



	f^*	μ_k^*	$m_{\mu k}^*$	\mathbb{R}
 3SDO	2350	● 1.00 ● 0.10	● 0.16 ● 0.15	3
 MTOP	2645	● 0.48	● 0.69	6025

Table 5: Mechanical compliance problem—Comparison of the computational cost.

	Step	# iter.	# feval
 3SDO	1. Conceptual	64	64
	2. Clustering	3	0
	3a. Sampling	30	30
	3b. Optimization	3	3
 MTOP	Outer	480	0
	Inner	1440	2880

6.3 Minimum Penetration and Mass under a Dynamic Load on an Armor Plate

Let us consider the thickness (topometry) optimization of an armor plate impacted by a rigid ball (Fig. 10). The plate undergoes large displacement and plasticity. Nonlinear finite element analysis is utilized. The goal is to minimize both the impact penetration and the mass of the plate. The dimension of the plate is 300 mm \times 300 mm. The displacement of the plate is constrained along its four edges. In the numerical analysis, the plate is discretized into 30 \times 30 identical finite elements. The rigid ball impacts the plate in a perpendicular direction at a speed of 10 m/s. The base material properties are listed in Table 6. The initial design has uniformly element thickness distribution of 5 mm as shown in Fig. 10. The initial design has maximum penetration $f_1 = 12.05$ mm and mass $f_2 = 0.50$.

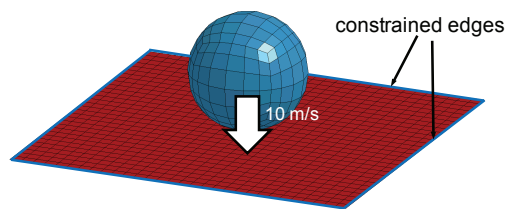


Fig. 10: Armor plate problem—Finite element model.

Step 1: Conceptual design The simulation is performed using explicit nonlinear finite element analysis in LS-DYNA. The conceptual design is obtained with one iteration of the HCA algorithm using element internal energy as the field variable [39]. The result is shown in Fig. 12. The contour indicates the value of the element thickness from 1 mm (white) to 10 mm (black). The average thickness is kept at 5 mm. The corresponding penetration is $f_1 = 9.33$ mm and the mass fraction is $f_2 = 0.50$.

Step 2: Clustered design The conceptual design is clustered using the K-means algorithm. A parametric study is

Table 6: Armor plate problem—Base material properties.

Property	Value	
Density	7830	kg/m ³
Elastic Modulus	207	GPa
Poisson's Ratio	0.3	
Yield stress	200	MPa
Tangent modulus	2.0	GPa

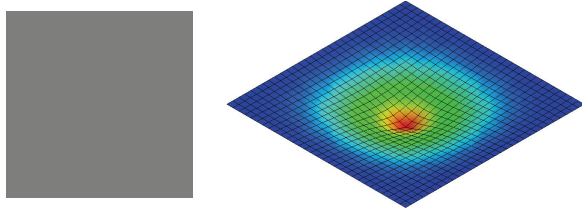


Fig. 11: Armor plate problem—Initial design (left) and impact simulation (right) with maximum penetration $f_1 = 12.05$ mm and mass fraction $f_2 = 0.50$.

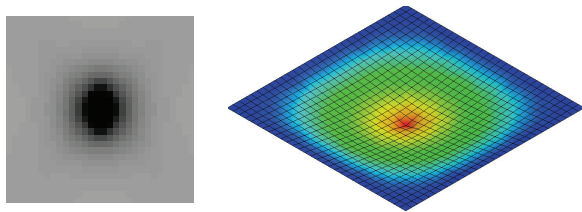


Fig. 12: Armor plate problem—Conceptual design (left) and impact simulation(right) with maximum penetration $f_1 = 9.33$ mm and mass fraction $f_2 = 0.50$.

performed to determine the influence of the K value. Figure 13 shows the clustered designs corresponding to $K = 1, \dots, 18$. Figure 14 shows the values of the the maximum penetration f_1 and mass fraction f_2 for each clustered design. As the number of clusters increases, the value of f_1 tends to decrease. The value of f_2 remains relatively constant. For the clustered design, it is desirable to keep the lowest K value and the lowest values for f_1 and f_2 . From these results, $K = 4$ can be identified as a potential optimal design.

Step 3: Metamodel-based global optimization The objective is to minimize both the maximum penetration f_1 and the mass fraction f_2 of the armor plate. The multi-objective

optimization problem is:

$$\begin{aligned}
 & \text{find } \boldsymbol{\mu} \in \mathbb{R}^K (K = 3) \\
 & \text{minimize } f_1(\mathbf{x}(\boldsymbol{\mu})) : \text{maximum penetration} \\
 & \text{minimize } f_2(\mathbf{x}(\boldsymbol{\mu})) : \text{mass fraction} \\
 & \text{subject to } 1 \leq \mu_k \leq 10, \quad k = 1, 2, 3.
 \end{aligned} \tag{18}$$

A Kriging metamodel is only required for f_1 . The number of LHS samples to build the f_1 initial metamodel is ten times the number of clusters, this is: $P = 10K$. The mass fraction function f_2 is linear and no metamodel is required; therefore, $\sigma_2 = 0$ and the multi-objective expected improvement Eq. (11) can be simplified to $E[I]$ as defined by Eq. (9).

The Pareto front of all clustered designs is shown in Fig. 15. As observed, Pareto designs for $K = 4$ dominates most of the other Pareto designs as well as the initial design, the conceptual design, and clustered design ($K = 4$). In this objective space, the conceptual design and the clustered design ($K = 4$) are close to each other. The computational cost of this structural optimization problem is summarized in Table 7.

Table 7: Armor plate problem—Computational cost of the 3SDO method ($K = 4$).

Step	# iter.	# feval
1. Conceptual	0	1
2. Clustering	12	0
3a. Sampling	40	40
3b. Optimization	100	100

6.4 Thin-walled S-rail crashworthiness design

Thin-walled S-rails are essential components of the progressive crushing zone in a vehicle. During a frontal or rear collision, S-rails are designed to absorb a high amount of the impact kinetic energy through plastic deformation. In this example, the geometry of the thin-walled S-rail of square cross section is defined as shown in Fig. 16, where $L = 1.0$ m. The S-rail is crushed in the axial direction by a rigid wall traveling at a constant speed of 5 m/s. The crushing distance is prescribed to be $0.5L$, which occurs 100 ms after the impact.

The objective is to maximize specific energy absorption (energy absorption per unit mass) and minimize peak crushing force. The design variable in this example is the shell element thickness of the S-rail. The material properties are summarized in Table 8.

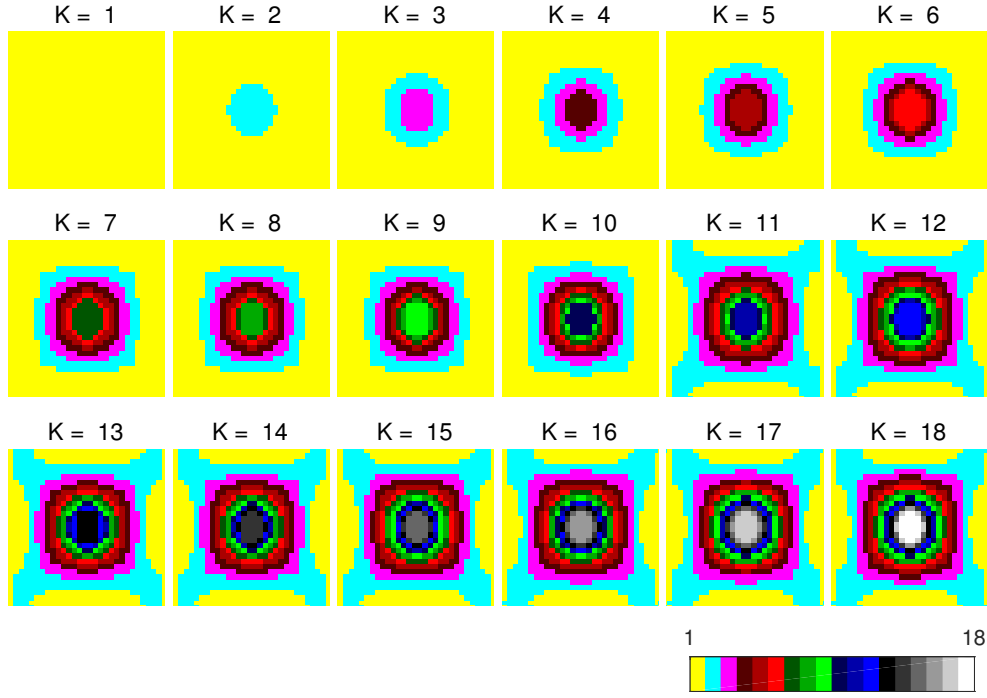


Fig. 13: Armor plate problem—Clustered designs with $K = 1, \dots, 18$.

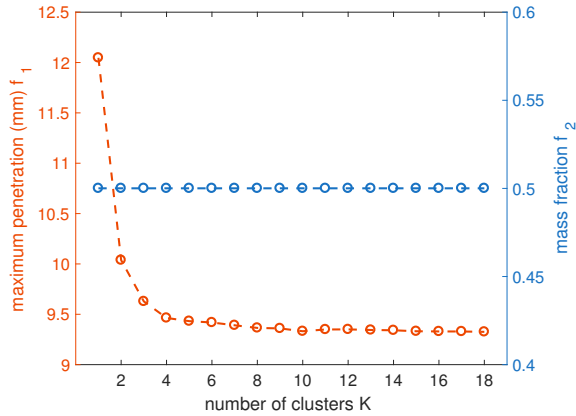


Fig. 14: Armor plate problem—Maximum penetration and mass fraction as functions of the number of clusters.

The crashworthiness indicators of the S-rail are the specific energy absorption (SEA) the peak crushing force (PCF). These crashworthiness indicators are defined as follows:

$$\text{SEA}(\mathbf{x}) = \frac{\int_{\delta} P(\mathbf{x}, \delta) d\delta}{m(\mathbf{x})}, \quad (19)$$

$$\text{PCF}(\mathbf{x}) = \max_{\delta} P(\mathbf{x}, \delta), \quad (20)$$

where $P(\mathbf{x}, \delta)$ is the reaction force of the thin-walled component at a crushed distance δ . The simulation is performed with the non-linear finite element analysis software LS-DYNA.

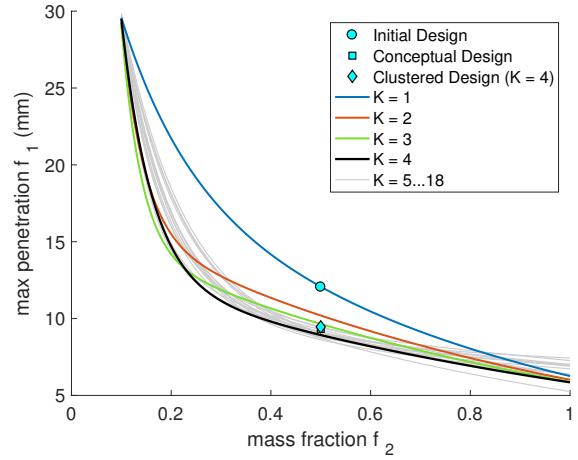


Fig. 15: Armor plate problem—Pareto front of the design optimization problem and the optimized clustered design ($K = 4$) with maximum penetration $f_1 = 9.46$ mm and mass fraction $f_2 = 0.50$.

Step 1: Conceptual design The conceptual design of the S-rail aims to trigger its progressive collapse. To this end, principles of compliant mechanism design are utilized: given the displacement of input ports, the objective is to find the thickness distribution that maximizes the displacement of output ports [3]. In this case, the input ports are prescribed at the contact nodes with a rigid wall. The output ports are defined by the wavelength λ of the progressive buckling corresponding to an ideal axial crushing condition [64] (Fig. 17). The optimization is to maximize the mutual potential energy

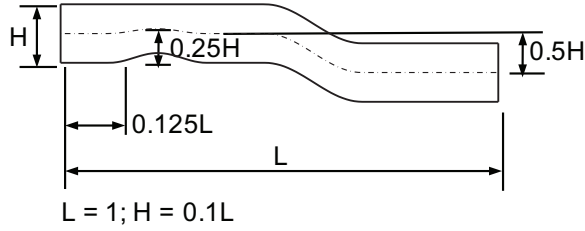


Fig. 16: S-rail problem—Geometry of the thin-walled S-rail (side view). The cross section is squared of dimensions $H \times H$ and thickness x_e .

Table 8: S-rail problem—Material properties of the finite element model.

Property	Value	
Density	7800	kg/m ³
Elastic Modulus (E)	207	GPa
Poisson's Ratio	0.29	
Yield stress (σ_Y)	253	MPa
Tangent modulus		
($\sigma_Y/E < \epsilon \leq 0.048$)	2437	MPa
($0.048 < \epsilon \leq 0.108$)	883	MPa
($0.108 < \epsilon \leq 0.148$)	550	MPa
($0.148 < \epsilon \leq 0.208$)	433	MPa
($0.208 < \epsilon \leq 0.407$)	281	MPa
($0.407 < \epsilon \leq 0.607$)	185	MPa
($0.607 < \epsilon \leq 0.987$)	124	MPa

of the structure subjected to a mass constraint [65]. This is:

$$\begin{aligned}
 & \text{find } \mathbf{x} \in \mathbb{R}^n \\
 & \text{minimize } f(\mathbf{x}, \mathbf{U}(\mathbf{x})) = -\mathbf{L}^T \mathbf{U}(\mathbf{x}) \\
 & \text{subject to } h(\mathbf{x}) = \frac{1}{n} \sum_{e=1}^n x_e - m_f = 0 \\
 & \quad x_e^L \leq x_e \leq x_e^U, \quad e = 1, \dots, n
 \end{aligned} \tag{21}$$

where \mathbf{x} is the thickness distribution, $\mathbf{U}(\mathbf{x})$ is the nodal displacement vector, and \mathbf{L} is the nodal (dummy) force vector with zeros at all degrees of freedom except for the ones corresponding to the output ports where the value is one. The lower thickness bound is $x_e^L = 0.6$ mm and the upper thickness bound is $x_e^U = 6.0$ mm. The mass fraction is set to be $m_f = 0.50$. The initial design has a constant thickness of 3.0 mm for all the finite elements. The corresponding

crash simulation shows Euler-type buckling with two plastic hinges (Fig. 18). The conceptual design is obtained with one iteration of the HCA algorithm using element mutual potential energy as the field variable [39]. Progressive folding is observed in this conceptual design. The corresponding thickness distribution and crash simulation are shown in Fig. 19.

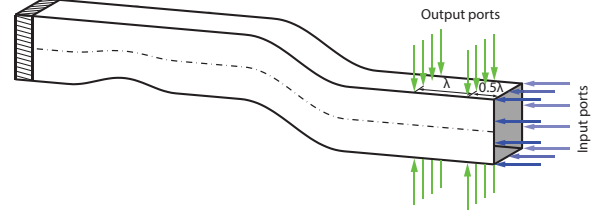


Fig. 17: S-rail problem—Locations of input and output ports for a thin-walled S-Tube following the wavelength λ corresponding to the progressive buckling after an ideal axial crushing condition.

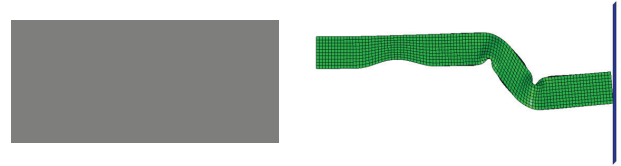


Fig. 18: S-rail problem—Initial design represented by a uniform thickness distribution in the “unfolded” thin-walled structure (left). The initial design depicts Euler-type buckling (right). The corresponding crashworthiness indicators are SEA= 3.39 kJ/kg and PCF= 267 kN.

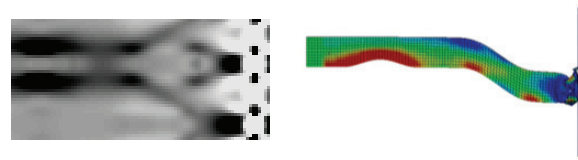


Fig. 19: S-rail problem—Conceptual design represented the thickness distribution in the “unfolded” thin-walled structure (left). The conceptual design depicts progressive folding (right). The corresponding crashworthiness indicators are SEA= 5.05 kJ/kg and PCF= 359 kN.

Step 2: Clustered design A parametric study is performed on the number of clusters. Figure 20 shows the “unfolded” clustered designs for $K = 1, \dots, 12$. The corresponding specific energy absorption (SEA) and peak crushing force (PCF) values are summarized in Figure 21. While a rigorous

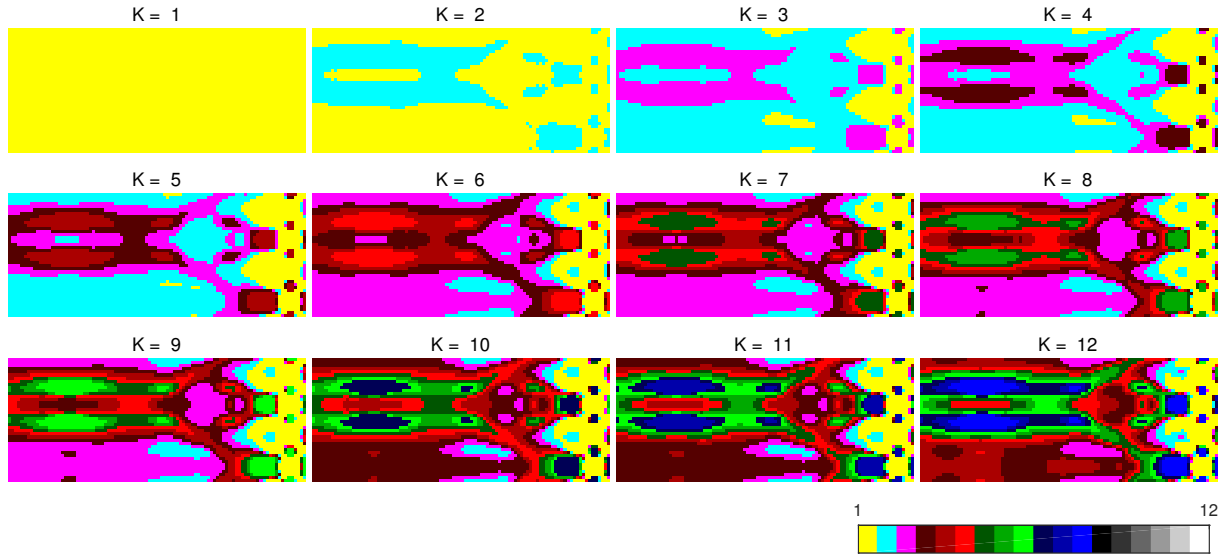


Fig. 20: S-rail problem—Clustered designs with $K = 1, \dots, 12$.

method to find the optimal number of K has not yet been found, in this example $K = 2$ depicts a desirable high SEA and low PCF values. This design can be identified as the potential optimal design.

lows:

$$\begin{aligned}
 & \text{find } \boldsymbol{\mu} \in \mathbb{R}^K \\
 & \text{maximize } \text{SEA}(\mathbf{x}(\boldsymbol{\mu})) \\
 & \text{minimize } \text{PCF}(\mathbf{x}(\boldsymbol{\mu})) \\
 & \text{subject to } 0.6 \text{ mm} \leq \mu_k \leq 6.0 \text{ mm}, \quad k = 1, \dots, K,
 \end{aligned} \tag{22}$$

where μ_k is the thickness of the k th cluster. Kriging meta-models are built for both objective functions using 40 initial LHS samples. The EGO algorithm with multi-objective expected improvement is utilized. Figure 22 shows the resulting Pareto front for $K = 1, \dots, 4$. All Pareto fronts dominate the initial design, the conceptual design, and clustered designs. The best clustered design is for $K = 2$; however, the best Pareto fronts correspond to $K = 3$ and $K = 4$. Table 9 summarizes the computational cost.

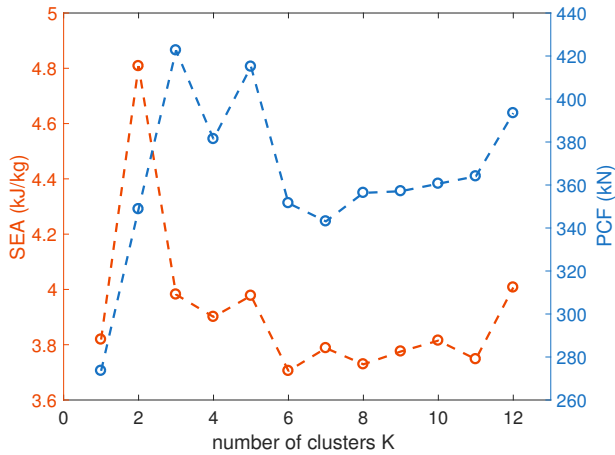


Fig. 21: S-rail problem—SEA and PCF values as a function of the number of clusters K .

Table 9: S-rail problem—3SDO computational cost

step	# iter.	# feval
Conceptual	1	2
Clustering	8	0
Sampling	40	40
Optimization	100	100

Step 3: Metamodel-based global optimization The design objectives are to maximize the specific energy absorption (SEA) and minimize the peak crushing force (PCF). The multi-objective optimization problem can be stated as fol-

7 Summary and Discussion

This work presents a design strategy to solve multi-material structural optimization problems that consists of

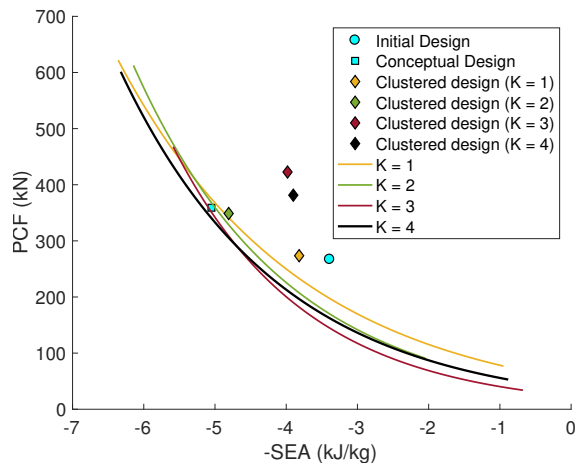


Fig. 22: S-rail problem—Pareto fronts for $K = 1, \dots, 4$. Initial, conceptual, and clustered design are dominated. Clustered designs have the following $(-SEA, PCF)$ coordinates: for $K = 1$: $(-3.82, 274)$, for $K = 2$: $(-4.81, 349)$, for $K = 3$: $(-3.98, 423)$, and for $K = 4$: $(-3.90, 381)$.

three steps: conceptual design generation, clustering, and metamodel-based global optimization. The conceptual design is a continuous design variable distribution generated by structural optimization in linear models (Secs. 6.1 and 6.2) or a heuristic design method such as HCA for nonlinear models (Secs. 6.3 and 6.4). Unsupervised machine learning techniques such as the K-means clustering algorithm are utilized to reduce the dimension of the optimization problem from thousands of design variables to a lower number of clusters. With the reduced number of design variables, metamodel-based global optimization can be performed. To this end, this work uses EGO. The proposed method is demonstrated through four examples: thermal compliance minimization, mechanical compliance minimization, mass and impact penetration minimization, as well as specific energy absorption maximization with peak crushing force minimization. The first two examples use linear finite element models under a static load. The last two examples use nonlinear finite element models under a dynamic load.

Aspects of the proposed structural optimization approach can be modified to solve specific problems. For example, instead of using topology optimization as illustrated in the paper, topography optimization can be applied. For clustering, K-means can be replaced by Principle Component Analysis or another unsupervised machine learning algorithm. In any case, the designer can supervise the design clustering and select the final number of clusters (materials) depending on the type of metamodel used in the final optimization step and/or the manufacturing process of the optimized design. Our ongoing research explores the use of supervised clustering methods.

In this work, the results of the linear models are compared to a multimaterial topology optimization algorithm, demonstrating lower computational cost in the proposed algorithm. For the nonlinear model, the results for different

number of clusters are compared. While more research is needed, the parametric studies in this work show that the analysis (crash simulation) of the cluster designs is a suitable indicator to approximate the optimal number of clusters. Other approaches such as the elbow method, information criterion approach, and the Silhouette method [51] are computationally less expensive but not as effective as the parametric study shown in this work. Ongoing investigation aims to control the structural complexity of the clustered design generated by the proposed approach.

Acknowledgements

Honda R&D Americas supported this research effort. Any opinions, findings, conclusions, and recommendations expressed in this investigation are those of the writers and do not necessarily reflect the views of the sponsors.

References

- [1] Bendsøe, M. P., 1995. *Optimization of structural topology, shape and material*. New York: Springer.
- [2] Allaire, G., 2001. *Shape optimization by the homogenization method*. Springer, New York.
- [3] Sigmund, O., and Torquato, S., 1997. “Design of materials with extreme thermal expansion using a three-phase topology optimization method”. *Journal of the Mechanics and Physics of Solids*, **45**(6), pp. 1037–1067.
- [4] Sigmund, O., and Torquato, S., 1999. “Design of smart composite materials using topology optimization”. *Smart Materials and Structures*, **8**(3), pp. 365–379.
- [5] Gibiansky, L. V., and Sigmund, O., 2000. “Multiphase composites with extremal bulk modulus”. *Journal of the Mechanics and Physics of Solids*, **48**(3), pp. 461–498.
- [6] Bendsøe, M. P., 1989. “Optimal shape design as a material distribution problem”. *Structural and Multidisciplinary Optimization*, **1**(4), pp. 193–202.
- [7] Mlejnek, H., 1992. “Some aspects of the genesis of structures”. *Structural Optimization*, **5**(1-2), pp. 64–69.
- [8] Zhou, M., and Rozvany, G., 1991. “The COC algorithm, part II: Topological, geometrical and generalized shape optimization”. *Computer Methods in Applied Mechanics and Engineering*, **89**, pp. 309–336.
- [9] Bendsøe, M. P., and Sigmund, O., 1999. “Material interpolations in topology optimization”. *Archive of Applied Mechanics*, **69**, pp. 635–654.
- [10] Gao, T., and Zhang, W., 2011. “A mass constraint formulation for structural topology optimization with multiphase materials”. *International Journal for Numerical Methods in Engineering*, **88**(8), pp. 774–796.
- [11] Cui, M. T., and Chen, H. F., 2014. “An improved alternating active-phase algorithm for multi-material topology optimization problems”. *Applied Mechanics and Materials*, **635-637**(105).

- [12] Osher, S., and F., S., 2001. “Level set methods for optimization problem involving geometry and constraints: I. Frequencies of a two-density inhomogeneous drum”. *Journal of Computational Physics*, **17**(1), pp. 272–288.
- [13] Wang, M. Y., Wang, X., and Guo, D., 2003. “A level set method for structural topology optimization”. *Computer Methods in Applied Mechanics and Engineering*, **192**(1-2), pp. 227–246.
- [14] Allaire, G., Jouve, F., and Toader, A.-M., 2004. “Structural optimization using sensitivity analysis and a level-set method”. *Journal of Computational Physics*, **194**(1), pp. 363–393.
- [15] Allaire, G., and Castro, C., 2002. “Optimization of nuclear fuel reloading by the homogenization method”. *Structural and Multidisciplinary Optimization*, **24**(1), pp. 11–22.
- [16] Mei, Y., and Wang, X., 2004. “A level set method for structural topology optimization and its applications”. *Advances in Engineering Software*, **35**(7), pp. 415–441.
- [17] Wang, M. Y., and Wang, X., 2004. ““color” level sets: A multi-phase method for structural topology optimization with multiple materials”. *Computer Methods in Applied Mechanics and Engineering*, **193**(6-8), pp. 469–496.
- [18] Wang, M. Y., and Wang, X., 2005. “A level-set based variational method for design and optimization of heterogeneous objects”. *CAD Computer Aided Design*, **37**(3), pp. 321–337.
- [19] Dombre, E., Allaire, G., Pantz, O., and Schmitt, D., 2012. “Shape optimization of a Sodium Fast Reactor core”. In *CEMRACS’11: Multiscale Coupling of Complex Models in Scientific Computing*, Vol. 38, pp. 319–334.
- [20] Wei, P., and Wang, M. Y., 2009. “Piecewise constant level set method for structural topology optimization”. *International Journal for Numerical Methods in Engineering*, **78**(4), pp. 379–402.
- [21] Luo, Z., Tong, L., Luo, J., Wei, P., and Wang, M. Y., 2009. “Design of piezoelectric actuators using a multi-phase level set method of piecewise constants”. *Journal of Computational Physics*, **228**(7), pp. 2643–2659.
- [22] Hamza, K., Aly, M., and Hegazi, H., 2013. “A kriging-interpolated level-set approach for structural topology optimization”. *Journal of Mechanical Design*, **136**(1), 11, pp. 011008–011008–12.
- [23] Guirguis, D., Hamza, K., Aly, M., Hegazi, H., and Saitou, K., 2015. “Multi-objective topology optimization of multi-component continuum structures via a kriging-interpolated level set approach”. *Structural and Multidisciplinary Optimization*, **51**(3), pp. 733–748.
- [24] Yoshimura, M., Shimoyama, K., Misaka, T., and Obayashi, S., 2017. “Topology optimization of fluid problems using genetic algorithm assisted by the kriging model”. *International Journal for Numerical Methods in Engineering*, **109**(4), pp. 514–532. nme.5295.
- [25] Chopp, D., 1993. “Computing minimal surface via level set curvature flow”. *Journal of Computational Physics*, **106**, pp. 77–91.
- [26] Sussman, M., Smereka, P., and Osher, S., 1994. “A level set approach for computing solutions to incompressible two-phase flow”. *Journal of Computational Physics*, **114**, pp. 146–159.
- [27] Sethian, J. A., 1999. *Level set methods and fast marching methods: evolving interfaces in computational geometry, fluid mechanics, computer vision and materials science*. Cambridge University Press, Cambridge, UK.
- [28] Osher, S., and Fedkiw, R., 2002. *Level Set Methods and Dynamic Implicit Surfaces*. Springer, New York.
- [29] Bourdin, B., and Chambolle, A., 2003. “Design-dependent loads in topology optimization”. *ESAIM: Control, Optimisation and Calculus of Variations*, **9**, pp. 19–48.
- [30] Wang, M. Y., and Zhou, S., 2005. “Synthesis of shape and topology of multi-material structures with a phase-field method”. *Journal of Computer-Aided Materials Design*, **11**(2-3), pp. 117–138.
- [31] Bourdin, B., and Chambolle, A., 2006. “The phase-field method in optimal design”. *IUTAM Symposium on Topological Design Optimization of Structures, Machines and Materials*, pp. 207–215.
- [32] Takezawa, A., Nishiwaki, S., and Kitamura, M., 2010. “Shape and topology optimization based on the phase field method and sensitivity analysis”. *Journal of Computational Physics*, **229**, pp. 2697–2718.
- [33] Blank, L., Garcke, H., Sarbu, L., and Styles, V., 2013. “Primal-dual active set methods for Allen–Cahn variational inequalities with nonlocal constraints”. *Numerical Methods for Partial Differential Equations*, **29**(3), pp. 999–1030.
- [34] Tavakoli, R., 2014. “Multimaterial topology optimization by volume constrained Allen–Cahn system and regularized projected steepest descent method”. *Computer Methods in Applied Mechanics and Engineering*, **276**(0), pp. 534–565.
- [35] Huang, X., and Xie, Y. M., 2009. “Bi-directional evolutionary topology optimization of continuum structures with one or multiple materials”. *Computational Mechanics*, **43**(3), pp. 393–401.
- [36] Huang, X., and Xie, M., 2010. *Evolutionary topology optimization of continuum structures: methods and applications*. John Wiley & Sons, Chichester, UK.
- [37] Lund, E., and Stegmann, J., 2005. “On structural optimization of composite shell structures using a discrete constitutive parametrization”. *Wind Energy*, **8**(1), pp. 109–124.
- [38] Stegmann, J., and Lund, E., 2005. “Discrete material optimization of general composite shell structures”. *International Journal for Numerical Methods in Engineering*, **62**(14), pp. 2009–2027.
- [39] Tovar, A., Patel, N. M., Niebur, G. L., Sen, M., and Renaud, J. E., 2006. “Topology optimization using a hybrid cellular automation method with local control rules”. *Journal of Mechanical Design, Transactions of the ASME*, **128**(6), pp. 1205–1216.
- [40] Tovar, A., Patel, N. M., Kaushik, A. K., and Renaud, J. E., 2007. “Optimality conditions of the hybrid cel-

- lular automata for structural optimization”. *AIAA Journal*, **45**(3), pp. 673–683.
- [41] Goetz, J., Tan, H., Renaud, J., and Tovar, A., 2012. “Two-material optimization of plate armour for blast mitigation using hybrid cellular automata”. *Engineering Optimization*, **44**(8), pp. 985 – 1005.
- [42] Holmberg, E., Torstenfelt, B., and Klarbring, A., 2013. “Stress constrained topology optimization”. *Structural and Multidisciplinary Optimization*, **48**(1), pp. 33–47.
- [43] Ishikawa, T., Nakayama, K., Kurita, N., and Dawson, F. P., 2014. “Optimization of rotor topology in pm synchronous motors by genetic algorithm considering cluster of materials and cleaning procedure”. *IEEE Transactions on Magnetics*, **50**(2), Feb, pp. 637–640.
- [44] Ishikawa, T., Mizuno, S., and Krita, N., 2017. “Topology optimization method for asymmetrical rotor using cluster and cleaning procedure”. *IEEE Transactions on Magnetics*, **53**(6), June, pp. 1–4.
- [45] Aulig, N., and Olhofer, M., 2016. “State-based representation for structural topology optimization and application to crashworthiness”. In 2016 IEEE Congress on Evolutionary Computation (CEC), pp. 1642–1649.
- [46] Liu, K., Tovar, A., and Detwiler, D., 2014. “Thin-walled component design optimization for crashworthiness using principles of compliant mechanism synthesis and Kriging sequential approximation”. In 4th International Conference on Engineering Optimization.
- [47] Hashin, Z., and Shtrikman, S., 1963. “A variational approach to the elastic behavior of multiphase minerals”. *Journal of the Mechanics and Physics of Solids*, **11**(2), pp. 127–140.
- [48] Wang, Y.-J., Zhang, J.-S., and Zhang, G.-Y., 2007. “A dynamic clustering based differential evolution algorithm for global optimization”. *European Journal of Operational Research*, **183**(1), pp. 56 – 73.
- [49] Xu, H., Chuang, C.-H., and Yang, R.-J., 2015. “A data mining-based strategy for direct multidisciplinary optimization”. *SAE Int. J. Mater. Manf.*, **8**, 04, pp. 357–363.
- [50] MacQueen, J. B., 1967. “Some methods for classification and analysis of multivariate observations”. In 5-th Berkeley Symposium on Mathematical Statistics and Probability, Vol. 1, University of California Press, pp. 281–297.
- [51] Liu, K., Tovar, A., Nutwell, E., and Detwiler, D., 2015. “Thin-walled compliant mechanism component design assisted by machine learning and multiple surrogates”. In SAE World Congress.
- [52] MacKay, D., 2003. *Information Theory, Inference, and Learning Algorithms*. Cambridge University Press, Cambridge, UK.
- [53] Bandi, P., Schmiedeler, J. P., and Tovar, A., 2013. “Design of crashworthy structures with controlled energy absorption in the hybrid cellular automaton framework”. *Journal of Mechanical Design*, **135**(091002), pp. MD–12–1267.
- [54] Lophaven, S. N., Nielsen, H. B., and Sondergaard, J., 2002. “dace”—a “matlab” kriging toolbox. Tech. rep., Informatics and Mathematical Modelling, Technical University of Denmark.
- [55] Myers, R., and Montgomery, D., 1995. *Response Surface Methodology. Process and Product Optimization using Designed Experiments*. Wiley.
- [56] Owen, A. B., 1994. “Controlling Correlations in Latin Hypercube Samples”. *Journal of the American Statistical Association*, **89**(428), dec, pp. 1517–1522.
- [57] Johnson, M., Moore, L., and Ylvisaker, D., 1990. “Minimax and maximin distance designs”. *Journal of Statistical Planning and Inference*, **26**(2), pp. 131–148.
- [58] Jones, D. R., Schonlau, M., and Welch, W. J., 1998. “Efficient global optimization of expensive black-box functions”. *Journal of Global Optimization*, **13**, pp. 455–492.
- [59] Viana, F. A. C., Haftka, R. T., and Steffen, V., 2009. “Multiple surrogates: how cross-validation errors can help us to obtain the best predictor”. *Structural and Multidisciplinary Optimization*, **39**(4), pp. 439–457.
- [60] Forrester, A. I. J., Sobester, A., and Keane, A. J., 2008. *Engineering Design via Surrogate Models*. JohnWiley & Sons, Chichester, UK.
- [61] Tavakoli, R., and Mohseni, S. M., 2014. “Alternating active-phase algorithm for multimaterial topology optimization problems: A 115-line MATLAB implementation”. *Structural and Multidisciplinary Optimization*, **49**(4), pp. 621–642.
- [62] Liu, K., and Tovar, A., 2014. “An efficient 3D topology optimization code written in Matlab”. *Structural and Multidisciplinary Optimization*, **50**(6), pp. 1175–1196.
- [63] Tovar, A., and Khandelwal, K., 2013. “Topology optimization for minimum compliance using a control strategy”. *Engineering Structures*, **48**, pp. 674 – 682.
- [64] Bandi, P., Detwiler, D., Schmiedeler, J. P., and Tovar, A., 2015. “Design of progressively folding thin-walled tubular components using compliant mechanism synthesis”. *Thin-Walled Structures*, **95**, pp. 208 – 220.
- [65] Saxena, A., and Ananthasuresh, G., 2000. “On an optimal property of compliant topologies”. *Structural and Multidisciplinary Optimization*, **19**(1), pp. 36–49.